

# PIO-FVLM: Rethinking Training-Free Visual Token Reduction for VLM Acceleration from an Inference-Objective Perspective

Haokui Zhang<sup>1</sup> Congyang Ou<sup>1</sup> Dawei Yan<sup>1</sup> Peng Wang<sup>1</sup> Qingsen Yan<sup>1</sup> Ying Li<sup>1</sup> Rong Xiao<sup>2</sup>  
Chunhua Shen<sup>3</sup>

## Abstract

Recently, reducing redundant visual tokens in vision-language models (VLMs) to accelerate VLM inference has emerged as a hot topic. However, most existing methods rely on heuristics constructed based on inter-visual-token similarity or cross-modal visual-text similarity, which gives rise to certain limitations in compression performance and practical deployment. In contrast, we propose PIO-FVLM from the perspective of inference objectives, which transforms visual token compression into preserving output result invariance and selects tokens primarily by their importance to this goal. Specially, vision tokens are reordered with the guidance of token-level gradient saliency generated by our designed layer-local proxy loss, a coarse constraint from the current layer to the final result. Then the most valuable vision tokens are selected following the non-maximum suppression (NMS) principle. The proposed PIO-FVLM is training-free and compatible with FlashAttention, friendly to practical application and deployment. It can be deployed independently as an encoder-free method, or combined with encoder compression approaches like VisionZip for use as an encoder-involved method. On LLaVA-Next-7B, PIO-FVLM retains just 11.1% of visual tokens but maintains 97.2% of the original performance, with a  $2.67\times$  prefill speedup,  $2.11\times$  inference speedup,  $6.22\times$  lower FLOPs, and  $6.05\times$  reduced KV Cache overhead. Our code is available at <https://github.com/ocy1/PIO-FVLM>.

## 1. Introduction

By incorporating visual information, vision-language models (VLMs) inherit the robust language reasoning capabilities of large language models (LLMs) while expanding their application scenarios, and have thus become a central focus of artificial intelligence research. Various VLMs have been proposed and achieved promising performance, such as Flamingo (Alayrac et al., 2022), BLIP-2 (Li et al., 2023a), LLaVA (Liu et al., 2023), and Qwen-VL (Bai et al., 2023). Nevertheless, although these VLMs enhance the functional performance of LLMs, they bring about considerable computational overhead in the meantime. Therefore, VLM acceleration has become a key problem.

Recently, a wealth of recent work focuses on compressing redundant tokens to reduce the computational cost and memory overhead while preserving model performance. Existing works fall into two main categories based on whether the vision encoder is involved in compression: *Vision Encoder-Involved(w/ VE)* and *Vision Encoder-Free(w/o VE)*. The former compresses visual tokens on the vision encoder side, reducing the length of the visual sequence before it is fed into the LLM, as exemplified by ToMe (Bolya et al., 2023), VisionZip (Yang et al., 2025b), HoloV (Zou et al., 2025), and SCOPE (Deng et al., 2025). The latter leaves the outputs of the vision encoder untouched and performs token selection directly within the LLM, with representative works including FastV (Chen et al., 2024), SparseVLM (Zhang et al., 2025b), and PyramidDrop (Xing et al., 2024).

Despite the progress made by the above methods, they still suffer from several limitations. Current methods have two major core ideas: 1) Attention map-based compression. Redundant tokens are filtered out by the importance of each token relative to others after the attention map is calculated in the self-attention module. Yet attention map computation accounts for the main computational cost of LLMs, so existing models usually adopt the FlashAttention mechanism (Dao et al., 2022) for iterative replacement to address this issue. However, full attention map-based methods suffer from poor compatibility with FlashAttention, which impairs the actual acceleration effect. 2) Similarity-based compression. Specifically, filtering is conducted by measuring the

<sup>1</sup>Northwestern Polytechnical University <sup>2</sup>Intellifusion Inc.  
<sup>3</sup>Zhejiang University. Correspondence to: Ying Li <lybyp1969@nwpu.edu.cn>.

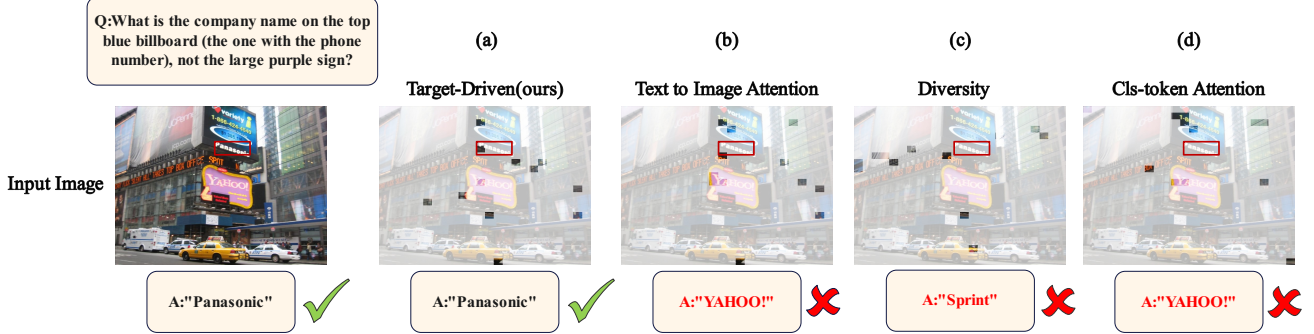


Figure 1. Comparison of different token selection strategies (selecting only 12 visual tokens as an example). (a) Ours; (b) Similirty with cls token and text token based; (c) cls token similarity based and enhance diversity; (d) Cls token similarity based.More examples are given in Appendix A.

similarity of visual tokens to the cls token (global token) (Fig.1(d)); the similarity among the selected tokens is also taken into account to ensure their diversity (Fig.1(c)); and a comprehensive metric is adopted by jointly considering the similarities of visual tokens to both the cls token and text tokens (Fig.1(b)). As shown in Fig.1, Mechanistically, all three of these methods carry the potential for misjudgment. Fig.1 (c)(d), The information encoded in the cls token is overly coarse and irrelevant to the input query, resulting in an incorrect final output. Fig.1(b), when text tokens are taken into account, the phrase the large purple sign in the query interferes with the judgment, leading to a bias toward "YAHOO!" on the purple sign.

We conjecture that both attention map-based and similarity-based methods select and filter visual tokens according to pre-defined rules, which may fail to cover all cases. Here, we rethink the VLM acceleration problem from an inferential perspective. From the perspective of preserving reasoning result consistency, we propose a training-free, FlashAttention-compatible visual feature compression method that enables plug-and-play integration into practical deployment for inference acceleration. Specifically, we design a highly simple layer-local proxy loss to roughly estimate the impact of vision tokens at any layer on preserving the current output. Based on this loss function, we derive the saliency of each vision token and then reorder vision tokens according to saliency. Furthermore, inspired by the NMS algorithm, we design an NMS-based selection algorithm to perform final selection on the reordered tokens. This operation is implemented in the LLM component, executed across multiple layers in a shallow-to-deep fashion with an increasingly intensive screening strength.

In summary, our contributions are three-fold:

- We present PIO-FVLM, a training-free visual token reduction method. To the best of our knowledge, this is the first goal-driven VLM acceleration method that does not rely solely on similarity or attention maps.

- Particularly, we design a layer-local proxy loss and an NMS selection method, both of which feature high computational efficiency and FlashAttention compatibility, enabling practical inference acceleration independent of code or hardware optimizations, as verified in Table 4.
- Experimental results on three popular VLMs and eight benchmarks verify the efficiency of PIO-FVLM.

## 2. Related Work

### 2.1. Multimodal Large Language Models.

Most VLMs follow a strong-LLM-centered paradigm with a vision module aligned to the LLM. Flamingo (Alayrac et al., 2022) connects frozen vision and language backbones via gated cross-attention for few-shot inference, while BLIP-2 (Li et al., 2023a) employs a Q-Former to align a frozen vision encoder with a frozen LLM efficiently. LLaVA (Liu et al., 2023) builds multimodal assistants via visual instruction tuning, and Qwen-VL (Bai et al., 2023) systematizes both architecture and training. This line further expands to open-source and video-capable models such as MiniGPT-4 (Zhu et al., 2023), InstructBLIP (Dai et al., 2023), Video-ChatGPT (Maaz et al., 2024), and Video-LLaVA (Lin et al., 2024). Gemini (Team et al., 2023) represents natively multimodal foundation models and achieves strong results on multimodal benchmarks. FlashAttention (Dao et al., 2022), as a highly efficient acceleration technique, has been widely adopted by these methods.

### 2.2. Visual Token Compression for VLMs.

Existing compression methods can be grouped by where they operate: *w/ VE* and *w/o VE*. *w/ VE* approaches compress within the vision encoder or at the decoder(LLM) interface, e.g., ToMe merges tokens by feature similarity (Bolya et al., 2023), VisionZip selects representative

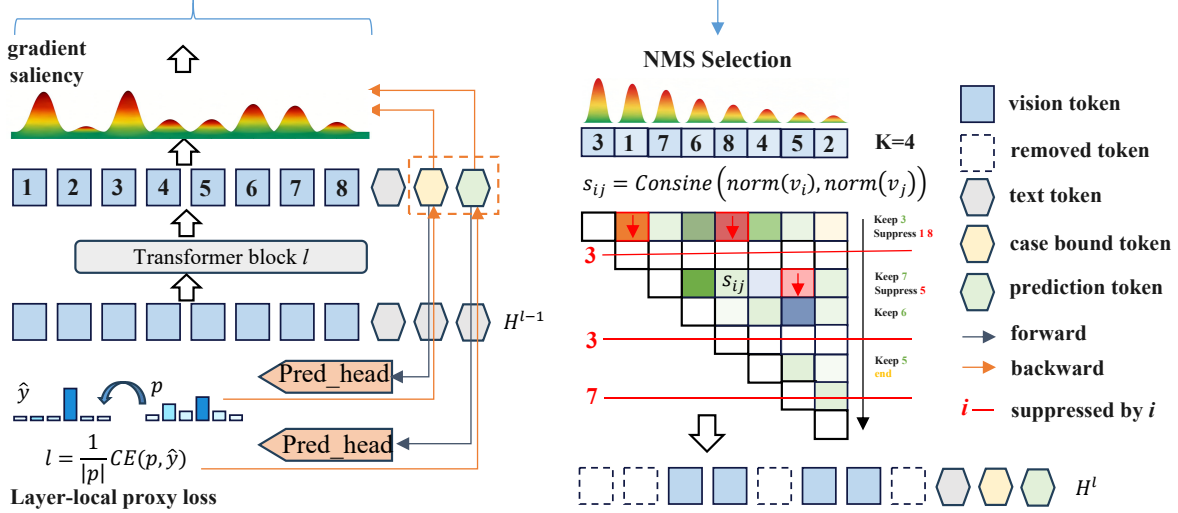


Figure 2. The architecture of PIO-FVLM. The overall framework consists of two stages. As shown on the left, the first stage is responsible for reordering vision tokens according to gradient saliency. The right side illustrates the second stage, which selects tokens based on the proposed NMS strategy. The *Pred\_head* is a pre-trained component native to the model, a prediction head originally designed to operate on the final-layer features.

tokens by CLS similarity (Yang et al., 2025b), HoloV (Zou et al., 2025), SCOPE (Deng et al., 2025), DivPrune (Alvar et al., 2025) and CDPruner (Zhang et al., 2025a) combine attention cues with spatial coverage for early compression. In contrast, w/ VE approaches prune tokens inside the decoder, including FastV (Chen et al., 2024) prunes to Top-K visual tokens ranked by text-to-image attention scores. SparseVLM (Zhang et al., 2025b) prunes visual tokens in-LLM using key-text attention scoring. Pyramid-Drop (Xing et al., 2024) progressively drops redundant visual tokens across LLM stages using text-to-image attention scores. TopV (Yang et al., 2025a), DART (Wen et al., 2025) and PACT (Dhouib et al., 2025) that further reduce deep-layer overhead via redundancy modeling or clustering-based merging. PIO-FVLM belongs to the W/O VE category, but owing to its flexibility, it can also be easily combined with methods such as VisionZip to form W/VE-type methods. Both modes are experimentally validated in this paper.

### 3. Method

In this section, we explain the principles and detailed design of PIO-FVLM in detail. First, we introduce its underlying logic, and then we describe the specific architecture of the method.

We know that the gradient magnitude of each token reflects the importance of the token in driving the model toward the ground-truth output (Selvaraju et al., 2017). As a straightforward extension, if we treat gradients as saliency to guide token selection and retain tokens with high saliency, we can basically ensure that the model output still converges to the ground truth. In other words, we derive the token

selection strategy in a reverse manner from the perspective of guaranteeing output performance.

There are two key challenges in generating such a gradient signal: 1) how to construct a computationally efficient loss function; 2) what constitutes the ground truth for the loss function. It is infeasible to construct a precise loss function that meets the required criteria, as this would require inference to the final layer, thus negating the purpose of acceleration. As shown in the left side of Fig.2, we propose the layer-local-proxy loss as a coarse approximation. Gradient-guided selection alone results in a lack of diversity in the selected tokens. Inspired by the NMS algorithm, we design an NMS selection algorithm to perform token selection based on gradient signal. We next elaborate on the design in the form of mathematical expressions.

#### 3.1. Problem Formulation

We consider a multimodal model with a vision encoder and an LLM decoder. Given an image  $I$  and instruction  $X$ , the encoder outputs visual tokens  $V = Enc(I)$ , which are projected as  $\tilde{V} = Proj(V)$  and concatenated with text embeddings  $T$  to form the decoder input  $H^{(0)} = [\tilde{V}; T]$ . The  $L$ -layer decoder updates.

$$H^l = f^l(H^{l-1}), \quad l = 1, \dots, L, \quad (1)$$

where  $l$  is the layer number,  $f^l$  means the transformer block of the  $l$ -th layer. During the prefill stage, we select several pruning layers for compression from shallow to deep, with the number of retained tokens decreasing progressively.

### 3.2. Layer-local Proxy Loss and Gradient Saliency

At each pruning layer  $l_{prune}$ , we first compute the layer-local proxy loss using the following formula:

$$L^l = \frac{1}{|\mathcal{P}^l|} \sum_{t \in \mathcal{P}^l} \text{CE}(p_t^l, \hat{y}_t^l), \quad (2)$$

where  $\text{CE}(\cdot, \cdot)$  denotes the standard cross-entropy loss.  $\mathcal{P}^l$  is the set of indices for tokens used in loss calculation.  $p_t^l$  and  $\hat{y}_t^l$  are soft logit and hard logit, which are calculated with formulas:

$$\begin{aligned} Z^l &= \text{Head}(\text{Norm}(H^l)), \\ p_t^l &= \text{softmax}(z_t), \\ \hat{y}_t^l &= \arg \max_i p_t^l(i), \end{aligned} \quad (3)$$

where  $\text{Head}$  denotes the original prediction head, used in the final layer of the original LLM. Here, we leverage it to generate soft logits.  $z_t$  is the  $t$ -th token in  $Z^l$ .  $\text{Norm}$  is the original layer normalization function of layer  $l$ . Here, we present two rough estimates as follows:

- Using shallow-layer features instead of the final-layer features to compute the loss. To mitigate the errors caused by the discrepancies between shallow and deep-layer features, our token pruning is implemented in a gradual manner. Only a small number of tokens are pruned at the shallow layer for high fault tolerance, while more tokens are pruned at the deep layer. Furthermore, this rough estimate converges increasingly to the accuracy result (using the final layer features) as the feature layer deepens. As verified by the visualization in Fig. 3.
- Generating hard logit  $\hat{y}_t^l$  as pseudo label. There is no ground truth available during the inference process, where hard logits are used as a substitute. This essentially validates the current outputs, informing the model that its current outputs are correct and that token pruning should be performed in a way that preserves these outputs.

Referring to Fig. 2,  $\mathcal{P}^l$  generally indicates the last few tokens in the sequence, the length of which is denoted as  $K_{pos}$ . In the prefill stage, text tokens follow vision tokens, with access to all vision tokens and preceding text tokens. Selecting end tokens enables full use of all token information. Additionally, we divide the selected tokens into case bound and prediction tokens by their functions. The last token generates the first answer token and constrains consistent answer generation, thus being the prediction token. Modifying the prefill stage code to generate more answer tokens would make this constraint more accurate, which is beyond

the scope of this paper and left for future research. The other tokens do not predict answers but constrain pruning to better adapt to the current case, hence being case bound tokens.

After obtaining the loss  $L^l$ , we perform a single-layer backward pass only with respect to the input hidden states  $H^{l-1}$  of the pruning layer and compute their gradients:

$$G^{l-1} = \frac{\partial L^l}{\partial H^{l-1}}. \quad (4)$$

We then compute the  $\ell_2$ -norm of the gradient vector for each token and use it as the gradient saliency score of that token at layer  $l$ :

$$s_i^l = \|G_i^{l-1}\|_2, \quad (5)$$

where,  $s_i^l$  measures how sensitive the layer-local proxy loss  $L^l$  is to a local perturbation of the  $i$ -th token. With our tail-window design, the final position provides an intent-alignment signal, while the preceding tail positions provide a case-coverage signal, yielding an objective-driven saliency that balances contextual coverage and generation direction.

Importantly, this procedure does not modify attention operators. We only run the standard forward of the pruning layer, attach the original output head, and compute gradients with respect to  $H^{l-1}$  in the usual way. Hence, the method is agnostic to the attention implementation and remains unchanged under standard attention or optimized kernels such as FlashAttention, making it fully compatible with high-efficiency attention backends in practice.

### 3.3. Gradient-based Visual Token Selection with NMS

In Sec. 3.2, we obtain gradient saliency scores  $\{s_i^l\}$  at pruning layer  $l$ . Under a given budget  $K$ , PIO-FVLM selects tokens that are *important yet non-redundant* from the target compression interval. Naive Top- $K$  by  $s_i^l$  often yields locally clustered high-score tokens, reducing global coverage under a fixed budget. To mitigate this, we apply feature-space non-maximum suppression (NMS) on top of gradient ranking to balance *objective relevance* and *diversity*.

Specifically, for each sample, we extract the score vector  $s$  within the compression interval and sort tokens in descending order to obtain the candidate sequence  $order$ . We then gather the corresponding token features  $v_j$  from the same interval, taken from the pruning layer input which is the previous layer hidden states, and apply  $\ell_2$  normalization.

$$u_j = \frac{v_j}{\|v_j\|_2}. \quad (6)$$

We then iteratively compute an extremely sparse upper triangular similarity matrix, the element of which is:

$$S_{ij} = \langle u_i, u_j \rangle. \quad (7)$$

Table 1. Performance comparison of different token reduction methods on LLaVA-1.5-7B under multiple token budgets. Both w/o VE and w/ VE versions achieve the best results

| Type                             | Methods             | Venue      | GQA  | MMB  | MMB-cn | MME    | POPE | SQA  | VQAv2 | TextVQA | Average      |
|----------------------------------|---------------------|------------|------|------|--------|--------|------|------|-------|---------|--------------|
| Baseline                         | <b>LLaVA-1.5-7B</b> | –          | 61.9 | 64.7 | 58.1   | 1862   | 85.9 | 69.5 | 78.5  | 58.2    | <b>100%</b>  |
| <b>Upper Bound, 576 Tokens</b>   |                     |            |      |      |        |        |      |      |       |         |              |
| w/o VE                           | Vanilla             | ECCV’24    | 52.7 | 61.2 | 57.0   | 1612   | 64.8 | 67.3 | 67.1  | 52.5    | 89.0%        |
| <b>Retain 192 Tokens (33.3%)</b> |                     |            |      |      |        |        |      |      |       |         |              |
| w/o VE                           | FastV               | CVPR’25    | 57.1 | 63.2 | 56.8   | 1766   | 82.3 | 68.8 | 75.1  | 56.1    | 96.2%        |
| w/o VE                           | PDrop               | ICML’25    | 59.5 | 64.1 | 53.7   | 1787   | 85.3 | 68.7 | 75.6  | 57.8    | 97.2%        |
| w/o VE                           | SparseVLM           | EMNLP’25   | 60.0 | 63.6 | 57.0   | 1856   | 82.8 | 69.8 | 76.7  | 57.4    | 98.3%        |
| w/o VE                           | DART                | Ours       | 61.0 | 64.4 | 57.6   | 1789   | 86.5 | 69.0 | 77.7  | 57.2    | <b>98.8%</b> |
| w/ VE                            | VisionZip           | CVPR’25    | 59.3 | 63.0 | 57.3   | 1782   | 85.3 | 68.9 | 76.8  | 57.3    | 97.8%        |
| w/ VE                            | HoloV               | NeurIPS’25 | 59.0 | 65.4 | 58.0   | 1820   | 85.6 | 69.8 | 76.7  | 57.4    | 98.7%        |
| w/ VE                            | SCOPE               | NeurIPS’25 | 60.1 | 63.6 | 56.8   | 1804   | 86.4 | 68.8 | 77.2  | 57.7    | 98.3%        |
| w/ VE                            | PIO-FVLM (Ours)     | Ours       | 61.1 | 64.2 | 57.9   | 1808   | 86.4 | 68.2 | 77.9  | 57.4    | <b>98.9%</b> |
| <b>Retain 128 Tokens (22.2%)</b> |                     |            |      |      |        |        |      |      |       |         |              |
| w/o VE                           | FastV               | ECCV’24    | 49.6 | 56.1 | 56.4   | 1490   | 59.6 | 60.2 | 61.8  | 50.6    | 83.2%        |
| w/o VE                           | PDrop               | CVPR’25    | 56.0 | 61.1 | 56.6   | 1644   | 82.3 | 68.3 | 72.9  | 55.1    | 94.0%        |
| w/o VE                           | SparseVLM           | ICML’25    | 58.4 | 64.5 | 51.1   | 1746   | 85.0 | 68.6 | 73.8  | 56.7    | 95.6%        |
| w/o VE                           | DART                | EMNLP’25   | 58.7 | 63.2 | 57.5   | 1840   | 80.1 | 69.1 | 75.9  | 56.4    | 97.0%        |
| w/o VE                           | PIO-FVLM (Ours)     | Ours       | 60.0 | 62.9 | 57.1   | 1807   | 86.7 | 68.5 | 76.5  | 57.2    | <b>98.1%</b> |
| w/ VE                            | VisionZip           | CVPR’25    | 57.6 | 62.0 | 56.7   | 1761.7 | 83.2 | 68.9 | 75.6  | 56.8    | 96.4%        |
| w/ VE                            | HoloV               | NeurIPS’25 | 57.7 | 63.9 | 56.5   | 1802   | 84.0 | 69.8 | 75.5  | 56.8    | 97.2%        |
| w/ VE                            | SCOPE               | NeurIPS’25 | 59.7 | 62.5 | 56.9   | 1776   | 86.1 | 68.4 | 76.5  | 57.2    | 97.5%        |
| w/ VE                            | PIO-FVLM (Ours)     | Ours       | 60.0 | 62.9 | 56.7   | 1799   | 86.4 | 69.2 | 77.1  | 57.0    | <b>98.1%</b> |
| <b>Retain 64 Tokens (11.1%)</b>  |                     |            |      |      |        |        |      |      |       |         |              |
| w/o VE                           | FastV               | ECCV’24    | 46.1 | 48.0 | 52.7   | 1256   | 48.0 | 51.1 | 55.0  | 47.8    | 74.0%        |
| w/o VE                           | PDrop               | CVPR’25    | 41.9 | 33.3 | 50.5   | 1092   | 55.9 | 68.6 | 69.2  | 45.9    | 74.4%        |
| w/o VE                           | SparseVLM           | ICML’25    | 53.8 | 60.1 | 52.7   | 1589   | 77.5 | 69.8 | 68.2  | 53.4    | 90.6%        |
| w/o VE                           | DART                | EMNLP’25   | 55.9 | 60.6 | 53.2   | 1765   | 73.9 | 69.8 | 72.4  | 54.4    | 92.8%        |
| w/o VE                           | PIO-FVLM (Ours)     | Ours       | 58.0 | 61.6 | 53.7   | 1681   | 84.3 | 68.5 | 74.8  | 54.9    | <b>94.7%</b> |
| w/ VE                            | VisionZip           | CVPR’25    | 55.1 | 60.1 | 55.4   | 1690   | 77.0 | 69.0 | 72.4  | 55.5    | 93.0%        |
| w/ VE                            | HoloV               | NeurIPS’25 | 55.3 | 63.3 | 55.1   | 1715   | 80.3 | 69.5 | 72.8  | 55.4    | 94.4%        |
| w/ VE                            | SCOPE               | NeurIPS’25 | 58.3 | 61.7 | 54.4   | 1698   | 83.9 | 68.6 | 75.3  | 56.6    | 95.4%        |
| w/ VE                            | PIO-FVLM (Ours)     | Ours       | 58.3 | 61.6 | 56.5   | 1744   | 86.4 | 68.6 | 75.9  | 56.2    | <b>96.6%</b> |

Given a threshold  $\tau$ , we regard two tokens as highly similar in feature space when  $S_{ij} \geq \tau$ , and treat them as redundant neighbors.

Based on gradient ranking and this adjacency relation, we adopt a **two-stage selection strategy**. We first perform *strict NMS*: candidates are scanned in *order*; if a candidate is not suppressed, it is added to the selected set  $\mathcal{S}$ , and all its neighbors with similarity above  $\tau$  are suppressed. The process stops once  $|\mathcal{S}|$  reaches the budget  $K$ , prioritizing high-gradient tokens while preventing feature-space clustering.

If  $|\mathcal{S}| < K$  after strict NMS, we apply *gradient completion* by filling the remaining slots with the highest-ranked unsuplected candidates following *order* until the budget is met.

This avoids under-selection under a high similarity threshold and ensures full budget utilization. The corresponding Algorithm is presented in Appendix D.

This design is motivated by two points: (i) gradient saliency directly reflects each token’s contribution to the output objective, while naive Top- $K$  tends to concentrate on locally high-response regions; and (ii) NMS explicitly removes redundancy via feature similarity, yielding better coverage and more stable selection under the same budget. Finally, the procedure is token-type agnostic, it may also be used to filter out text tokens, a point that will be verified in future work.

Table 2. Performance comparison of different token reduction methods on LLaVA-NeXT-7B under multiple token budgets. Blue-highlighted rows denote our method.

| Method               | Venue      | GQA  | MMBench | MMBench-cn | MME  | POPE | SQA  | VQAv2 | TextVQA | Avg          |
|----------------------|------------|------|---------|------------|------|------|------|-------|---------|--------------|
| <b>LLaVA-NeXT-7B</b> |            |      |         |            |      |      |      |       |         |              |
| Vanilla              | –          | 64.2 | 67.4    | 60.6       | 1851 | 86.5 | 70.1 | 81.8  | 61.4    | 100%         |
| <b>LLaVA-NeXT-7B</b> |            |      |         |            |      |      |      |       |         |              |
| FastV                | ECCV’24    | 55.9 | 61.6    | 51.9       | 1661 | 71.7 | 62.8 | 71.9  | 55.7    | 88.1%        |
| SparseVLM            | ICML’25    | 56.1 | 60.6    | 54.5       | 1533 | 82.4 | 66.1 | 71.5  | 58.4    | 90.3%        |
| VisionZip            | CVPR’25    | 59.3 | 63.1    | 55.6       | 1702 | 82.1 | 67.3 | 76.2  | 58.9    | 93.7%        |
| CDPruner             | NeurIPS’25 | 61.6 | 65.5    | 55.7       | 1453 | 87.2 | 67.8 | 78.4  | 57.4    | 93.8%        |
| DART                 | EMNLP’25   | 61.7 | 65.3    | 58.2       | 1710 | 84.1 | 68.4 | 79.1  | 58.7    | 96.1%        |
| HoloV                | NeurIPS’25 | 61.7 | 65.3    | 57.5       | 1738 | 83.9 | 68.9 | 79.5  | 58.7    | 96.2%        |
| PIO-FVLM (Ours)      | Ours       | 61.8 | 66.2    | 59.5       | 1795 | 84.5 | 68.9 | 79.3  | 58.3    | <b>97.2%</b> |

### 3.4. Theoretical Analysis

Following FastV (Chen et al., 2024), we count only the dominant matrix-multiplication costs in a Transformer block:

$$f(n) = 4nd^2 + 2n^2d + 2ndm, \quad (8)$$

where  $n$  is the sequence length,  $d$  is the hidden dimension, and  $m$  is the FFN intermediate dimension.

For a 32-layer LLaVA decoder, we prune at  $[1, 10, 15]$ , yielding  $[V_0, V_1, V_2, V_3]$  (effective from the next layer). The total FLOPs are

$$F_{\text{total}} = F_{\text{inf}} + F_{\text{ov}}, \quad (9)$$

where  $F_{\text{inf}}$  is the post-pruning inference cost and  $F_{\text{ov}}$  is the overhead(local gradients + feature-space NMS). Here  $\gamma$  is the compute factor of one local backward pass relative to a forward pass:

$$F_{\text{inf}} = f(V_0) + 9f(V_1) + 5f(V_2) + 17f(V_3), \quad (10)$$

$$F_{\text{ov}} = \gamma(f(V_0) + f(V_1) + f(V_2)). \quad (11)$$

The theoretical reduction ratio is

$$\text{Saved} = 1 - \frac{F_{\text{total}}}{32f(V_0)}. \quad (12)$$

A detailed proof is provided in Appendix C.

## 4. Experiments and Analysis

### 4.1. Experimental Setup

**Models and Baselines.** We evaluate PIO-FVLM on three LVLMs with diverse architectures: LLaVA-1.5 (Liu et al., 2023), LLaVA-NeXT (Liu et al., 2024a), and Qwen-2.5-VL (Bai et al., 2025). We compare against eight representative visual-token reduction baselines, including FastV (Chen et al., 2024), SparseVLM (Zhang et al., 2025b), Pyramid-Drop (Xing et al., 2024), VisionZip (Yang et al., 2025b), DART (Wen et al., 2025), HoloV (Zou et al., 2025), SCOPE (Deng et al., 2025), and CDPruner (Zhang et al., 2025a).

**Datasets.** We report image-based results on eight standard benchmarks: GQA (Hudson & Manning, 2019), MMBench, MMBench-CN (Liu et al., 2024b), MME (Fu et al., 2025), POPE (Li et al., 2023b), SQA (Lu et al., 2022), VQAV2 (Goyal et al., 2017), and TextVQA (Singh et al., 2019).

**Implementation Details.** We follow the default inference settings in the official codebases. Pruning layers are set to  $[1, 10, 15]$  for LLaVA models and  $[1, 8, 14]$  for Qwen models, with  $K_{\text{pos}} = 4$  and  $\tau = 0.8$ . Ablations are provided in Section 4.3.

### 4.2. Main Results

**Results on LLaVA-1.5.** We first apply PIO-FVLM to LLaVA-1.5, which is widely adopted for evaluating visual token pruning strategies. As shown in Table 1, PIO-FVLM achieves state-of-the-art performance across all budgets in **both w/ VE and w/o VE** settings. In the *w/o VE* track, it consistently outperforms competitors, retaining 98.8% and 94.7% average performance at 192 and 64 tokens respectively, surpassing DART (98.3% and 92.8%). Furthermore, the *w/ VE* setting elevates the SOTA to a higher level: it reaches 98.9% retention at 192 tokens and maintains 96.6% under the extreme 64-token regime, significantly outperforming the previous best Encoder-Involved method.

Notably, before the proposal of PIO-FVLM, *w/o VE* methods generally exhibited lower accuracy than *w/ VE* ones. Our *w/o VE* variant, by contrast, not only outperforms strong *w/o VE* baselines such as DART but also surpasses some existing *w/ VE* methods. Our *w/ VE* variant adopts a two-stage hybrid scheme: SCOPE-style pre-filtering (Deng et al., 2025) before token injection, followed by objective-driven refinement with PIO-FVLM at layer 16. This combines early efficiency with stronger deep-layer objective alignment, yielding better results than pre-filtering alone under the same budget.

**Results on LLaVA-NeXT.** To assess scalability on high-resolution architectures with denser visual tokens, we simu-

Table 3. Performance comparison of different token reduction methods on Qwen2.5-VL-7B under multiple token budgets. Blue-highlighted rows denote our method.

| Method             | Venue    | MMBench | MME  | POPE | SQA   | MMBench-cn | GQA   | TextVQA | Avg          |
|--------------------|----------|---------|------|------|-------|------------|-------|---------|--------------|
| <b>Qwen-2.5-VL</b> |          |         |      |      |       |            |       |         |              |
| Vanilla            | –        | 83.7    | 2299 | 87   | 88.65 | 81.8       | 61    | 77.7    | 100%         |
| <b>Qwen-2.5-VL</b> |          |         |      |      |       |            |       |         |              |
| DART               | EMNLP’25 | 80.9    | 2316 | 82.8 | 84.88 | 79.0       | 57.67 | 70.4    | 95.7%        |
| PIO-FVLM (Ours)    | Ours     | 82.1    | 2317 | 85.9 | 88.7  | 80.5       | 60.1  | 75.5    | <b>98.8%</b> |
| <b>Qwen-2.5-VL</b> |          |         |      |      |       |            |       |         |              |
| DART               | EMNLP’25 | 78.9    | 2227 | 80.4 | 84.2  | 76.5       | 55.76 | 67      | 92.8%        |
| PIO-FVLM (Ours)    | Ours     | 80.9    | 2284 | 85.4 | 88    | 78.1       | 58.8  | 74.4    | <b>97.3%</b> |
| <b>Qwen-2.5-VL</b> |          |         |      |      |       |            |       |         |              |
| DART               | EMNLP’25 | 73.3    | 1971 | 73.3 | 82    | 71.5       | 50.3  | 57.3    | 84.8%        |
| PIO-FVLM (Ours)    | Ours     | 77.6    | 2150 | 77.5 | 84.8  | 75.5       | 53.5  | 70.6    | <b>91.7%</b> |

Table 4. Efficiency and accuracy comparison of the baseline and our method (11.1% retention) across different models. We report prefill time, total inference time, FLOPs, KV cache, and POPE accuracy.

| Methods                       | Prefill Time $\downarrow$<br>(s)               | Total Time $\downarrow$<br>(s)                 | Avg FLOPs $\downarrow$<br>(T)                   | KV Cache $\downarrow$<br>(MB)                 | POPE<br>(Acc) |
|-------------------------------|--|--|---|---|---------------|
| LLaVA-1.5-7B<br>+Ours(%11.1)  | 1401 (1.00 $\times$ )<br>1106 (1.27 $\times$ ) | 2234 (1.00 $\times$ )<br>1978 (1.13 $\times$ ) | 2.98 (1.00 $\times$ )<br>0.45 (6.62 $\times$ )  | 318 (1.00 $\times$ )<br>62 (5.13 $\times$ )   | 85.9<br>84.3  |
| LLaVA-NeXT-7B<br>+Ours(%11.1) | 4934 (1.00 $\times$ )<br>1844 (2.67 $\times$ ) | 5921 (1.00 $\times$ )<br>2810 (2.11 $\times$ ) | 16.67 (1.00 $\times$ )<br>2.68 (6.22 $\times$ ) | 1156 (1.00 $\times$ )<br>191 (6.05 $\times$ ) | 86.5<br>84.5  |

late a resource-constrained setting by retaining 320 visual tokens on average per layer. As shown in Table 2, PIO-FVLM remains robust under this aggressive compression, achieving 96.5% SOTA average retention and surpassing HoloV (95.5%) and DART (95.4%), while substantially alleviating the severe degradation of FastV (87.5%) and SparseVLM (89.6%).

**Results on Qwen-2.5-VL.** Following the CDPruner protocol (Zhang et al., 2025a), we fix the input resolution to  $1008 \times 1008$  (1,296 visual tokens per image). As shown in Table 3, PIO-FVLM consistently outperforms DART across all pruning ratios, and the advantage becomes more pronounced at higher compression levels: at the aggressive 11.1% retention rate, PIO-FVLM maintains 91.7% average performance retention, exceeding DART (84.8%) by 6.9%. Overall, these results confirm that our inference-objective perspective robustly preserves discriminative semantics across diverse VLM backbones and token-density regimes.

### 4.3. Ablation Study and Analysis

**Runtime and Memory Evaluation.** In Table 4, we evaluate the practical acceleration effects of **PIO-FVLM**. By retaining only **11.1%** of visual tokens, PIO-FVLM achieves a **1.13 $\times$**  speedup in overall inference and a **1.27 $\times$**  speedup

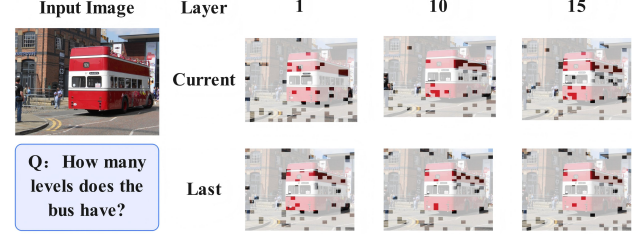
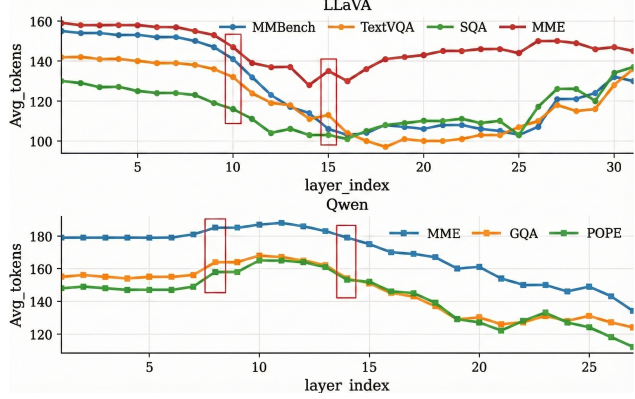


Figure 3. Visualization of selected important visual tokens (64 retained) using different gradient signals. Token selection is performed at Layers [1, 10, 15]: the top row (Current) ranks image tokens by gradients from the current-layer local proxy loss, while the bottom row (Last) uses gradients propagated from the final-layer output loss. Highlighted patches indicate the retained tokens.

in the prefill stage on **LLaVA-1.5-7B**, while maintaining robust POPE performance with only a slight drop (**85.9 $\rightarrow$ 84.3**). More significant acceleration is observed on **LLaVA-NeXT-7B**, where PIO-FVLM delivers a **2.11 $\times$**  speedup in total time and a **2.67 $\times$**  speedup during prefill, retaining competitive accuracy (**86.5 $\rightarrow$ 84.5**). In addition, PIO-FVLM effectively compresses KV-cache storage across different backbones, reducing it from **318MB** to **62MB** (**5.13 $\times$** ) on LLaVA-1.5-7B and from **1156MB** to **191MB** (**6.05 $\times$** ) on LLaVA-NeXT-7B. These results demonstrate that PIO-FVLM can substantially reduce inference overhead under an extreme token budget, while preserving robust visual reasoning performance. It is also important to note that PIO-FVLM is compatible with FlashAttention(Dao et al., 2022), which can further enhance efficiency.

**Rationale of Gradient-Based Token Selection.** Motivated by findings (Jain & Wallace, 2019) that attention weights can be weakly correlated with feature importance and can be perturbed with negligible output change, we adopt *gradient saliency* to measure each token’s influence via output sensitivity. Fig. 3 visualizes the selected **64** visual tokens at pruning Layers [1, 10, 15], comparing two importance sig-



**Figure 4. Layer-wise gradient saliency statistics.** For each benchmark and layer, we report the average number of tokens per question whose gradient scores exceed the layer-wise mean. Red boxes highlight layers exhibiting notable distribution shifts for LLaVA and Qwen.

nals: **Current** (layer-local gradients induced by a proxy loss at the current layer) and **Last** (global gradients backpropagated from the final output loss). As illustrated in Fig.3, two key phenomena can be observed:

- The guiding signals generated by the current layer exhibit a high degree of consistency with those from the last layer. Furthermore, in practice, given that Transformer blocks possess a global receptive field, tokens that are spatially adjacent exhibit high similarity. Thus, the selected tokens do not require strict alignment; approximate effects can be achieved as long as their covered regions are roughly similar.
- With increasing depth, the consistency of the guiding signals from the current layer and the last layer exhibits a gradual increase. This is quite intuitive: as the depth increases, the level of feature abstraction rises, and the features of the current layer become increasingly close to those of the last layer. This characteristic aligns perfectly with our design. At shallow layers, consistency exists but remains low, so we only remove a small number of vision tokens, resulting in a high fault tolerance. At deep layers, since the guiding signals become more accurate, we can eliminate more vision tokens.

## Hyperparameter Settings

**Pruning-layer selection strategy.** Guided by the layer-wise gradient-saliency curves in Fig. 4, which illustrate the average number of tokens per layer whose gradient scores exceed the mean, we prune at Layers [1, 10, 15] for LLaVA and Layers [1, 8, 14] for Qwen.

This selection is primarily based on two principles:

- Pruning is performed as early as possible in the net-

**Table 5. Ablation on  $K_{\text{pos}}$  (Avg scores on different benchmarks).** All settings use the same pruning configuration (LLaVA-v1.5-7B, tokens=64); higher is better.

| $K_{\text{pos}}$ | 1     | 2     | 3     | 4     | 5     | 6     | 7     | 8     |
|------------------|-------|-------|-------|-------|-------|-------|-------|-------|
| Avg              | 92.1% | 94.6% | 94.6% | 94.9% | 94.9% | 94.8% | 94.7% | 94.8% |

**Table 6. Ablation on NMS and  $\tau$  Avg scores on different benchmarks.** All settings use the same pruning configuration (llava-v1.5-7B, tokens=64) (higher is better).

| $\tau$ | 0.70  | 0.75  | 0.80  | 0.85  | 0.90  | 0.95  | no nms |
|--------|-------|-------|-------|-------|-------|-------|--------|
| Avg    | 94.6% | 94.7% | 94.8% | 94.4% | 94.2% | 93.6% | 92.1%  |

work, as this most effectively reduces computational overhead and achieves acceleration. Therefore, all selected pruning layers lie in the first half of the network.

- We select layers with drastic gradient changes, as such layers exhibit sharp variations in token information, and this is exactly when tokens need to be selected carefully.

**$K_{\text{pos}}$  selection.** As shown in Table 5, the choice of  $K_{\text{pos}}$  substantially affects the stability and coverage of the proxy loss. Using only the last position ( $K_{\text{pos}}=1$ ) yields a sparse supervision signal and results in a much lower average accuracy (92.1%). Once a few preceding positions are included ( $K_{\text{pos}}=2 \sim 5$ ), the proxy loss both aligns with the immediate output objective and better covers the current instance, leading to a large performance jump and a stable plateau. In particular,  $K_{\text{pos}}=4$  achieves the best average accuracy (94.9%), offering a more reasonable trade-off between objective alignment and contextual robustness. Further increasing  $K_{\text{pos}}$  provides diminishing returns and can slightly degrade performance, suggesting that too many positions may introduce noisier and less focused gradient signals.

**NMS and threshold choice.** As shown in Table 6, applying feature-space cosine-similarity NMS consistently improves performance over the Top- $K$  baseline without NMS. As the threshold  $\tau$  increases, suppression becomes weaker: overly small  $\tau$  may over-prune and discard useful evidence, while overly large  $\tau$  fails to remove redundant, highly similar tokens and degenerates toward Top- $K$  behavior. Empirically,  $\tau = 0.8$  yields the best average accuracy (94.8%), suggesting a better trade-off between reducing redundancy for broader coverage and preserving critical information.

## 5. Conclusion

This paper presents PIO-FVLM, a training-free VLM acceleration method. It for the first time breaks the limitation of such methods heavily relying on attention maps or similarity metrics, leveraging gradient saliency to guide visual

token selection. It frames token compression as output invariance preservation, using a custom layer-local proxy loss for gradient saliency-guided token reordering, and is FlashAttention-compatible.

## References

Alayrac, J.-B., Donahue, J., Luc, P., Miech, A., Barr, I., Hasson, Y., Lenc, K., Mensch, A., Millican, K., Reynolds, M., et al. Flamingo: a visual language model for few-shot learning. *Advances in neural information processing systems*, 35:23716–23736, 2022.

Alvar, S. R., Singh, G., Akbari, M., and Zhang, Y. Divprune: Diversity-based visual token pruning for large multimodal models. In *Proceedings of the Computer Vision and Pattern Recognition Conference*, pp. 9392–9401, 2025.

Bai, J., Bai, S., Yang, S., Wang, S., Tan, S., Wang, P., Lin, J., Zhou, C., and Zhou, J. Qwen-vl: A frontier large vision-language model with versatile abilities. *arXiv preprint arXiv:2308.12966*, 1(2):3, 2023.

Bai, S., Chen, K., Liu, X., Wang, J., Ge, W., Song, S., Dang, K., Wang, P., Wang, S., Tang, J., et al. Qwen2. 5-vl technical report. *arXiv preprint arXiv:2502.13923*, 2025.

Bolya, D., Fu, C.-Y., Dai, X., Zhang, P., Feichtenhofer, C., and Hoffman, J. Token merging: Your vit but faster. In *The Eleventh International Conference on Learning Representations*, 2023.

Chen, L., Zhao, H., Liu, T., Bai, S., Lin, J., Zhou, C., and Chang, B. An image is worth 1/2 tokens after layer 2: Plug-and-play inference acceleration for large vision-language models. In *European Conference on Computer Vision*, pp. 19–35. Springer, 2024.

Dai, W., Li, J., Li, D., Tiong, A., Zhao, J., Wang, W., Li, B., Fung, P. N., and Hoi, S. Instructblip: Towards general-purpose vision-language models with instruction tuning. *Advances in neural information processing systems*, 36: 49250–49267, 2023.

Dao, T., Fu, D., Ermon, S., Rudra, A., and Ré, C. Flashattention: Fast and memory-efficient exact attention with io-awareness. *Advances in neural information processing systems*, 35:16344–16359, 2022.

Deng, J., Li, W., Zhou, J. T., and He, Y. Scope: Saliency-coverage oriented token pruning for efficient multimodel llms. *arXiv preprint arXiv:2510.24214*, 2025.

Dhouib, M., Buscaldi, D., Vanier, S., and Shabou, A. Pact: Pruning and clustering-based token reduction for faster visual language models. In *Proceedings of the Computer Vision and Pattern Recognition Conference*, pp. 14582–14592, 2025.

Fu, C., Chen, P., Shen, Y., Qin, Y., Zhang, M., Lin, X., Yang, J., Zheng, X., Li, K., Sun, X., et al. Mme: A comprehensive evaluation benchmark for multimodal large language models. In *The Thirty-ninth Annual Conference on Neural Information Processing Systems Datasets and Benchmarks Track*, 2025.

Goyal, Y., Khot, T., Summers-Stay, D., Batra, D., and Parikh, D. Making the v in vqa matter: Elevating the role of image understanding in visual question answering. In *Proceedings of the IEEE conference on computer vision and pattern recognition*, pp. 6904–6913, 2017.

Hudson, D. A. and Manning, C. D. Gqa: A new dataset for real-world visual reasoning and compositional question answering. In *Proceedings of the IEEE/CVF conference on computer vision and pattern recognition*, pp. 6700–6709, 2019.

Jain, S. and Wallace, B. C. Attention is not explanation. *arXiv preprint arXiv:1902.10186*, 2019.

Li, J., Li, D., Savarese, S., and Hoi, S. Blip-2: Bootstrapping language-image pre-training with frozen image encoders and large language models. In *International conference on machine learning*, pp. 19730–19742. PMLR, 2023a.

Li, Y., Du, Y., Zhou, K., Wang, J., Zhao, X., and Wen, J.-R. Evaluating object hallucination in large vision-language models. In *The 2023 Conference on Empirical Methods in Natural Language Processing*, 2023b.

Lin, B., Ye, Y., Zhu, B., Cui, J., Ning, M., Jin, P., and Yuan, L. Video-llava: Learning united visual representation by alignment before projection. In *Proceedings of the 2024 conference on empirical methods in natural language processing*, pp. 5971–5984, 2024.

Liu, H., Li, C., Wu, Q., and Lee, Y. J. Visual instruction tuning. *Advances in neural information processing systems*, 36:34892–34916, 2023.

Liu, H., Li, C., Li, Y., Li, B., Zhang, Y., Shen, S., and Lee, Y. J. Llavanext: Improved reasoning, ocr, and world knowledge, 2024a.

Liu, Y., Duan, H., Zhang, Y., Li, B., Zhang, S., Zhao, W., Yuan, Y., Wang, J., He, C., Liu, Z., et al. Mmbench: Is your multi-modal model an all-around player? In *European conference on computer vision*, pp. 216–233. Springer, 2024b.

Lu, P., Mishra, S., Xia, T., Qiu, L., Chang, K.-W., Zhu, S.-C., Tafjord, O., Clark, P., and Kalyan, A. Learn to explain: Multimodal reasoning via thought chains for science question answering. *Advances in Neural Information Processing Systems*, 35:2507–2521, 2022.

Maaz, M., Rasheed, H., Khan, S., and Khan, F. Video-chatgpt: Towards detailed video understanding via large vision and language models. In *Proceedings of the 62nd Annual Meeting of the Association for Computational Linguistics*, pp. 12585–12602, 2024.

Selvaraju, R. R., Cogswell, M., Das, A., Vedantam, R., Parikh, D., and Batra, D. Grad-cam: Visual explanations from deep networks via gradient-based localization. In *Proceedings of the IEEE international conference on computer vision*, pp. 618–626, 2017.

Singh, A., Natarajan, V., Shah, M., Jiang, Y., Chen, X., Batra, D., Parikh, D., and Rohrbach, M. Towards vqa models that can read. In *Proceedings of the IEEE/CVF conference on computer vision and pattern recognition*, pp. 8317–8326, 2019.

Team, G., Anil, R., Borgeaud, S., Alayrac, J.-B., Yu, J., Soricut, R., Schalkwyk, J., Dai, A. M., Hauth, A., Millican, K., et al. Gemini: a family of highly capable multimodal models. *arXiv preprint arXiv:2312.11805*, 2023.

Wen, Z., Gao, Y., Wang, S., Zhang, J., Zhang, Q., Li, W., He, C., and Zhang, L. Stop looking for important tokens in multimodal language models: Duplication matters more. *arXiv preprint arXiv:2502.11494*, 2025.

Xing, L., Huang, Q., Dong, X., Lu, J., Zhang, P., Zang, Y., Cao, Y., He, C., Wang, J., Wu, F., et al. Pyramid-drop: Accelerating your large vision-language models via pyramid visual redundancy reduction. *arXiv preprint arXiv:2410.17247*, 2024.

Yang, C., Sui, Y., Xiao, J., Huang, L., Gong, Y., Li, C., Yan, J., Bai, Y., Sadayappan, P., Hu, X., et al. Topv: Compatible token pruning with inference time optimization for fast and low-memory multimodal vision language model. In *Proceedings of the Computer Vision and Pattern Recognition Conference*, pp. 19803–19813, 2025a.

Yang, S., Chen, Y., Tian, Z., Wang, C., Li, J., Yu, B., and Jia, J. Visionzip: Longer is better but not necessary in vision language models. In *Proceedings of the Computer Vision and Pattern Recognition Conference*, pp. 19792–19802, 2025b.

Zhang, Q., Liu, M., Li, L., Lu, M., Zhang, Y., Pan, J., She, Q., and Zhang, S. Beyond attention or similarity: Maximizing conditional diversity for token pruning in mllms. *arXiv preprint arXiv:2506.10967*, 2025a.

Zhang, Y., Fan, C.-K., Ma, J., Zheng, W., Huang, T., Cheng, K., Gudovskiy, D. A., Okuno, T., Nakata, Y., Keutzer, K., and Zhang, S. SparseVLM: Visual token sparsification for efficient vision-language model inference. In *Forty-second International Conference on Machine Learning*, 2025b.

Zhu, D., Chen, J., Shen, X., Li, X., and Elhoseiny, M. Minigpt-4: Enhancing vision-language understanding with advanced large language models. *arXiv preprint arXiv:2304.10592*, 2023.

Zou, X., Lu, D., Wang, Y., Yan, Y., Lyu, Y., Zheng, X., Zhang, L., and Hu, X. “Don’t just chase” highlighted tokens” in mllms: Revisiting visual holistic context retention. *arXiv preprint arXiv:2510.02912*, 2025.

## Appendix

### A. Visual Comparison and Failure Mode Analysis of Four Token Selection Strategies

To reveal how different visual token reduction strategies affect the retained evidence, we compare four representative methods under the same input and the same token budget, as shown in Fig. 5. The four methods include objective driven selection, text to image attention based selection, diversity oriented selection, and CLS attention based selection. Each question corresponds to one row of results, where colored grids indicate the retained visual token locations, together with the predicted answers and correctness marks.

Overall, the objective driven method consistently allocates the limited budget to regions that are directly relevant to the question, such as key fragments of scene text, local areas required for spatial relation reasoning, and dense regions of objects for counting. As a result, it remains more stable on fine grained tasks that rely on precise evidence, including text reading and relative position judgment, object counting, and existence verification. In contrast, attention based heuristics can be biased toward globally salient regions or language priors, which may lead to insufficient coverage near the decisive evidence and thus systematic errors. The diversity oriented strategy provides broader spatial coverage, but it dilutes the sampling density over crucial regions under a fixed budget, making it prone to misses on fine grained recognition and counting. The CLS attention strategy behaves more like a global summary and is less targeted to local discriminative cues, which also causes failures on samples requiring high resolution evidence.

These cases suggest that visual token selection should consider not only relevance but also evidence usability and discriminability under a strict budget. By aligning token selection with the current output objective, the objective driven mechanism preserves more useful evidence at the same budget, leading to more reliable answers.

### B. Detailed Experiment Settings.

#### B.1. Datasets.

**GQA**(Hudson & Manning, 2019) is a large-scale dataset for visual question answering, where compositional questions are generated over structured scene graphs built from real images. Unlike conventional VQA benchmarks, GQA emphasizes systematic coverage of object attributes, relations, and their logical compositions, and is designed to reduce language priors via stricter annotations and question construction. It is widely used to evaluate fine-grained visual grounding and compositional reasoning in vision–language models.

**TextVQA**(Singh et al., 2019) is a visual question answering benchmark that focuses on scene text understanding, where answering often requires reading and reasoning over text visible in the image. It contains diverse natural images with text-rich content such as signs, packages, posters, and storefronts, encouraging the integration of OCR with visual–textual reasoning. Since answers are highly dependent on textual cues in the scene, TextVQA is widely used to evaluate scene text recognition, text grounding, and text-centric multimodal reasoning.

**ScienceQA**(Lu et al., 2022) is a multimodal question answering benchmark for scientific reasoning, covering multi-domain science problems from elementary to middle school levels. Instances are typically multiple-choice questions, with inputs including text and optionally images, aiming to test concept understanding, vision–language reasoning, and multi-step inference. ScienceQA is widely used to evaluate multimodal models on educational knowledge and structured reasoning.

**POPE**(Li et al., 2023b) is a benchmark for evaluating hallucinations in vision–language models, formulated as binary questions about whether a specific object actually appears in an image. By building matched positive and negative pairs under controlled conditions, it checks whether the model claims an object is present without visual support, allowing quantitative evaluation of object-level hallucination and visual faithfulness. POPE is commonly used to compare grounding quality and anti-hallucination robustness across VLMs.

**MME**(Fu et al., 2025) is a comprehensive benchmark for evaluating multimodal large language models, covering both perception and cognition tasks. Given an image and a short instruction or question, it assesses perceptual abilities such as object recognition, attribute and relation understanding, counting, and scene reasoning, as well as cognitive abilities including commonsense reasoning, logic, and knowledge understanding. MME is widely used for holistic evaluation and cross-model comparison of general multimodal capabilities.

**VQAV2**(Goyal et al., 2017) is a widely used large-scale visual question answering dataset, where a model predicts a short

answer given an image and a natural-language question. To mitigate language priors, VQAv2 introduces paired images for the same question that lead to different answers, encouraging models to rely on visual evidence rather than dataset biases. It is commonly used to evaluate fundamental visual understanding, vision–language alignment, and general VQA capability.

**MMBench**(Liu et al., 2024b) is a comprehensive evaluation benchmark for multimodal large language models, formulated as multiple-choice questions spanning diverse vision understanding and reasoning skills. Each instance typically includes an image and a textual query with several answer candidates, assessing capabilities such as object/attribute recognition, relation and spatial reasoning, counting, commonsense, and logical inference. With a unified option space and convenient automatic scoring, MMBench is widely used for fair cross-model comparison.

## B.2. Models.

**llava-1.5**(Liu et al., 2023) is a widely used vision–language instruction-following model that follows the standard “vision encoder + multimodal projector + LLM decoder” paradigm. It first tokenizes an image into visual tokens and extracts features with a vision encoder, projects them into the language embedding space, and then concatenates them with text tokens for joint decoding and generation. Trained with large-scale vision–language instruction data, LLaVA-1.5 provides robust performance on open-ended VQA, visual dialogue, and many multimodal benchmarks, making it a strong baseline for research on multimodal reasoning and visual token reduction.

**llava-next**(Liu et al., 2024a) is an upgraded vision–language model in the LLaVA family, targeting stronger general capability and better support for high-resolution inputs. It retains the standard “vision encoder + multimodal projector + LLM decoder” backbone while improving data curation, training strategies, and multimodal alignment. Compared to LLaVA-1.5, LLaVA-NeXT is more robust for complex instructions, multi-turn dialogue, and fine-grained visual understanding, and it better handles longer visual-token sequences induced by higher-resolution images, making it a stronger and more challenging baseline for acceleration and token reduction studies.

**qwen-2.5-vl**(Bai et al., 2025) is a multimodal large language model in the Qwen family, designed for general vision–language understanding and generation. It typically combines a vision encoder to extract image representations with multimodal alignment mechanisms that integrate visual features into the language model embedding space, enabling capabilities such as image QA, multimodal dialogue, OCR-centric understanding, and multi-step reasoning. With strong performance across many benchmarks and often long visual-token sequences under high-resolution inputs, Qwen-2.5-VL is widely used to evaluate the generalization of visual token reduction and inference acceleration methods.

## C. Theoretical Analysis

### C.1. Per-layer FLOPs and Baseline

We follow the FastV-style approximation and only count the dominant matrix-multiplication FLOPs within each Transformer block (self-attention + FFN):

$$f(n) = 4nd^2 + 2n^2d + 2ndm. \quad (13)$$

Without pruning, the token length remains  $V_0$  for all layers, yielding the baseline FLOPs

$$F_{\text{base}} = 32f(V_0). \quad (14)$$

### C.2. Backbone Inference FLOPs $F_{\text{inf}}$ (Pruning at 1/10/15, Layers 1–32)

Layers are indexed as  $1, \dots, 32$ . Pruning is performed at layers 1/10/15 and becomes effective from the next layer. Therefore, the four segments are: (i) layer 1: length  $V_0$  (1 layer); (ii) layers 2–10: length  $V_1$  (9 layers); (iii) layers 11–15: length  $V_2$  (5 layers); (iv) layers 16–32: length  $V_3$  (17 layers). Hence,

$$F_{\text{inf}} = f(V_0) + 9f(V_1) + 5f(V_2) + 17f(V_3). \quad (15)$$

### C.3. Local Gradient Overhead $F_{\text{grad}}$

At each pruning layer, we perform one extra forward pass of the current block to construct the proxy loss, and one backward pass to obtain the token-level input gradients. Let  $\beta$  denote the FLOPs ratio of the backward pass to the forward pass under

the same approximation. Then the overhead per pruning layer is approximately

$$(1 + \beta)f(V). \quad (16)$$

Since the three pruning stages occur when the current visual token lengths are  $V_0, V_1, V_2$  respectively, we obtain

$$F_{\text{grad}} = (1 + \beta)(f(V_0) + f(V_1) + f(V_2)). \quad (17)$$

Let  $\gamma = 1 + \beta$ , then

$$F_{\text{grad}} = \gamma(f(V_0) + f(V_1) + f(V_2)). \quad (18)$$

#### C.4. Total FLOPs and Reduction Ratio

The total overhead is

$$F_{\text{ov}} = F_{\text{grad}} + F_{\text{nms}} = \gamma(f(V_0) + f(V_1) + f(V_2)), \quad (19)$$

and the total FLOPs after pruning is

$$F_{\text{total}} = F_{\text{inf}} + F_{\text{ov}}. \quad (20)$$

Therefore, the reduction ratio is

$$\text{Saved} = 1 - \frac{F_{\text{total}}}{F_{\text{base}}} = 1 - \frac{F_{\text{inf}} + F_{\text{ov}}}{32f(V_0)}. \quad (21)$$

## D. Gradient-based Visual Token Selection with NMS

---

**Algorithm 1** Gradient-based Visual Token Selection with NMS
 

---

```

1: Input: Gradient saliency scores  $\mathbf{s} \in \mathbb{R}^N$ , Token features  $\mathbf{V} \in \mathbb{R}^{N \times d}$ , Budget  $k_{keep}$ , Threshold  $\tau$ .
2: Output: Selected token indices  $\mathcal{S}$ .
3: // 1. Pre-processing
4: Normalize features:  $\mathbf{u}_i \leftarrow \mathbf{v}_i / \|\mathbf{v}_i\|_2, \forall i \in \{1, \dots, N\}$ 
5: Sort candidates:  $\mathcal{O} \leftarrow \text{Argsort}(\mathbf{s}, \text{descending})$ 
6: Initialize selected set  $\mathcal{S} \leftarrow \emptyset$  and suppression mask  $\mathcal{M} \leftarrow \mathbf{0}^N$ 
7: // 2. Stage I: Strict NMS
8: for  $i$  in  $\mathcal{O}$  do
9:   if  $|\mathcal{S}| \geq k_{keep}$  then
10:    break
11:   end if
12:   if  $\mathcal{M}[i] = 0$  then
13:      $\mathcal{S} \leftarrow \mathcal{S} \cup \{i\}$ 
14:     // Compute similarity with all tokens
15:      $\mathbf{sim} \leftarrow \mathbf{U} \cdot \mathbf{u}_i^\top$ 
16:     // Suppress neighbors with high similarity
17:      $\mathcal{M} \leftarrow \mathcal{M} \vee (\mathbf{sim} \geq \tau)$ 
18:   end if
19: end for
20: // 3. Stage II: Gradient Completion (Fill remaining budget)
21: if  $|\mathcal{S}| < k_{keep}$  then
22:   for  $i$  in  $\mathcal{O}$  do
23:     if  $|\mathcal{S}| \geq k_{keep}$  then
24:       break
25:     end if
26:     if  $i \notin \mathcal{S}$  then
27:        $\mathcal{S} \leftarrow \mathcal{S} \cup \{i\}$ 
28:     end if
29:   end for
30: end if
31: return  $\mathcal{S}$ 
  
```

---

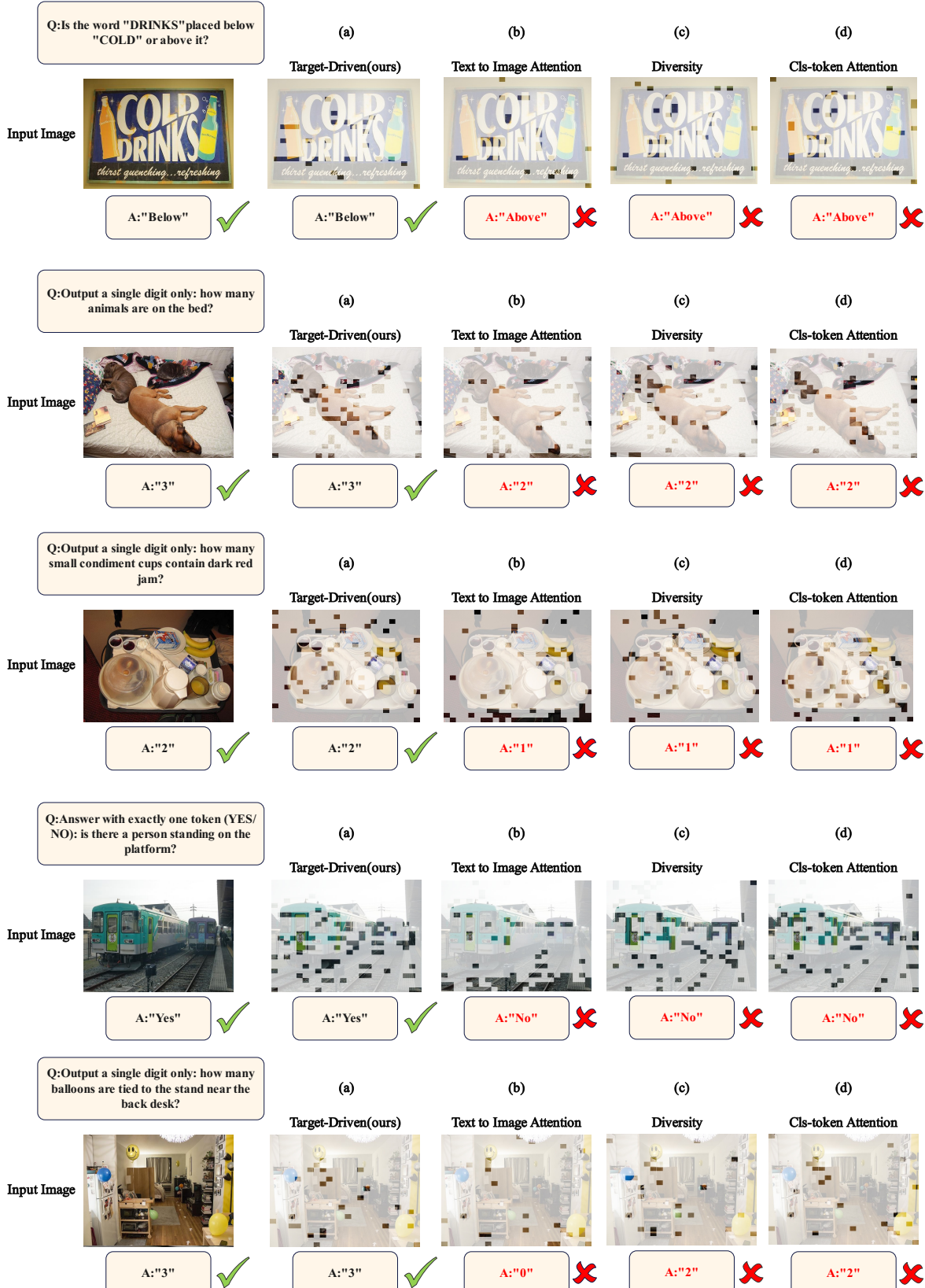


Figure 5. Comparison of different token selection strategies. (a) Ours; (b) Similarity with cls token and text token based; (c) cls token similarity based and enhance diversity; (d) Cls token similarity based.